

XMM-Newton Spectra of Intermediate-Mass Black Hole Candidates: Application of a Monte-Carlo Simulated Model

Q. Daniel Wang¹, Yangsen Yao¹, Wakako Fukui¹, ShuangNan Zhang², & Rosa Williams^{1,3}

ABSTRACT

We present a systematic spectral analysis of six ultraluminous X-ray sources (NGC1313 X-1/X-2, IC342 X-1, HoIX X-1, NGC5408 X-1 and NGC3628 X-1) observed with *XMM-Newton* Observatory. These extra-nuclear X-ray sources in nearby late-type galaxies have been considered as intermediate-mass black hole candidates. We have performed Monte-Carlo simulations of Comptonized multi-color black-body accretion disks. This unified and self-consistent spectral model assumes a spherically symmetric, thermal corona around each disk and accounts for the radiation transfer in the Comptonization. We find that the model provides satisfactory fits to the *XMM-Newton* spectra of the sources. The characteristic temperatures of the accretion disks (T_{in}), for example, are in the range of $\sim 0.05 - 0.3$ keV, consistent with the intermediate-mass black hole interpretation. We find that the black hole mass is typically about a few times $10^3 M_{\odot}$ and has an accretion rate $\sim 10^{-6} - 10^{-5} M_{\odot} \text{ yr}^{-1}$. For the spectra considered here, we find that the commonly used multi-color black-body accretion disk model with an additive power law component, though not physical, provides a good mathematical approximation to the Monte-Carlo simulated model. However, the latter model provides additional constraints on the properties of the accretion systems, such as the disk inclination angles and corona optical depths.

Subject headings: galaxies: general — galaxies: individual (NGC 1313, IC342, HoIX, NGC 5408 and NGC 628) — X-rays: general — X-rays: galaxies

1. Introduction

Probably the most exciting recent development in the field of black hole (BH) study is the discovery of numerous candidates for intermediate-mass BHs (IMBHs) with masses in

¹Department of Astronomy, University of Massachusetts, Amherst, MA 01003

²Department of Physics, University of Alabama, Huntsville, AL 35899

³Department of Astronomy, University of Illinois, Urbana, IL 61801

the range of $\sim 10^2 - 10^5 M_\odot$ (see Miller & Colbert 2003 for a recent review). The presence of such BHs was first proposed to explain ultraluminous X-ray sources (ULXs), defined as point-like extra-nuclear X-ray sources observed in nearby galaxies and with inferred isotropic X-ray luminosities in excess of 10^{39} erg s $^{-1}$, about an order of magnitude greater than the Eddington limit of a solar mass object (e.g., Fabbiano 1989; Colbert & Mushotzky 1999; Miller et al. 2003a,b; Strohmayer & Mushotzky 2003). While unambiguous detections of individual IMBHs currently do not exist, there are observational hints from studies of microlensing events, globular clusters, and centers of nearby galaxies (van der Marel 2003 and references therein). Although ULXs actually represent a heterogeneous population, a majority of them are likely to be accreting BHs. The controversy is centered on the X-ray emission mechanisms and on the masses of the BHs (e.g., Makishima et al. 2000; King et al. 2001; Begelman 2002).

The IMBH interpretation, though probably the most straightforward and exciting, has serious difficulties (e.g., King et al. 2001; Kubota et al. 2002). In addition to their high X-ray luminosities, many ULXs show convex-shaped spectra, especially in the energy band \lesssim a few keV. Such spectra are characteristic of the “soft state” of accreting BH binaries and are often approximated by black-body-like models such as the multi-color disk model (MCD; *diskbb* in the *XSPEC* spectral analysis software package (Arnaud 1996; e.g., Makishima et al. 1986). In the MCD model, each annulus of the axis-symmetric optically-thick accretion is assumed to radiate as a blackbody with a radius-dependent temperature. The characteristic temperature T_{in} of the innermost portion of the disk is $\propto (\dot{M}/M)^{1/4}$, where M and \dot{M} are the BH mass and the accretion mass rate. However, T_{in} inferred from the model fit is almost always too high for the required high mass, assuming the Eddington limit on \dot{M} . Equivalently, the inner disk radius R_{in} is much smaller than the last stable orbit for a non-spin BH. Even more disturbing is that the inferred value of R_{in} is sometimes found to be time-variable, in contrast to the soft-state of confirmed BH X-ray binaries, where R_{in} is approximately constant for each source.

Furthermore, it has been shown recently that many X-ray spectra of ULXs cannot be satisfactorily described by a single MCD model, especially in observations with good counting statistics and with a broad energy coverage (e.g., Miller et al. 2003a,b). The usual practice is then to fit such a spectrum with an additive combination of an MCD and a power law (PL; e.g, Miller 2003a,b; Cropper et al. 2003). The requirement of this latter component, which often becomes important at energies \gtrsim a few keV and may extend up to 200 keV as indicated by stellar mass BH systems, suggests that a high temperature electron cloud (corona) exists around an accretion disk, producing inverse-Compton scattering of the disk photons (e.g., Kubota et al. 2002; Page et al. 2003). A spectral fit with this additive, phenomenological model combination typically leads to an acceptable fit and a much lower (apparently more

reasonable) disk temperature. Nevertheless, the model is over-simplified in the following two aspects:

First, the extension of the power-law component straight to the low-energy limit of the spectrum is nonphysical. Because the power-law component is assumed to mimic the effect of the inverse Compton scattering, a low-energy cutoff as in the MCD component must be present in the Comptonized component (see also Page et al. 2003). Neglecting this low-energy cutoff could mis-characterize the spectral shape of the MCD component and could lead to an artificially high absorption in spectral fitting.

Second, the additive combination of the MCD and the PL components does not account for the radiative transfer process or the removal of photons from the MCD component to the Comptonized component. Furthermore, this process depends on both disk photon and corona electron energies. Therefore, one may not, in general, directly take the MCD normalization derived from the spectral model fitting to infer the inner disk radius or the BH mass, as realized by some authors (e.g., Kubota, Makishima & Ebisawa 2001). Otherwise, the inferred (but probably nonphysical) inner disk radius, for example, may appear to vary significantly when an accretion system changes from its hard state to its soft state or vice versa, as in XTE J2012+381 (Campana et al. 2002).

These oversimplifications in the MCD+PL model certainly obscure the physical dependence of the Comptonization on the corona and disk properties, and could also seriously affect the inference of accretion disk parameters.

Yao et al. (2003, hereafter Paper I) have recently developed a Comptonized multi-color disk (CMCD) model. They use Monte-Carlo simulations to directly generate the Comptonized X-ray spectra, removing the above mentioned over-simplifications and avoiding the complications of using the two (unrelated)-component model and then trying to correct for various radiative transfer effects. While the MCD model is still used to describe the accretion disk emission, the Comptonized radiation is no longer an independent component. This self-consistent treatment thus provides a new tool to constrain the physical properties of the corona and to study its relationship to the accretion disk. But most importantly, the model enables us to recover the same original disk flux in a spectral fit, which is essential to a reliable mass estimate of the putative BH.

In the present work, we apply the CMCD model to the analysis of *XMM-Newton* spectra of six ULXs which have been suggested as IMBH candidates. Our main objectives are to check whether or not the CMCD model provides an adequate spectral description of these sources and to see what potential new insights we may gain from such an application. The sources and data are described in §2, whereas the implementation of the model for this

application is discussed in §3, which also includes a summary of various corrections required to infer BH masses from the present model fits. We also test the PL, MCD, and MCD+PL models and compare them with the CMCD model. We present the results of our spectral fits in §4 and discuss the implications and conclusions in §5.

2. Selected ULXs and *XMM-Newton* Data

For our initial application of the CMCD model to the IMBH candidates, we concentrate on *XMM-Newton* X-ray observations of six previous known ULXs in nearby galaxies ($D \lesssim 10$ Mpc; Table 1). The moderate spatial resolution of *XMM-Newton* observations (e.g., FWHM $\sim 6''$ at 1 keV) is sufficient to isolate the emission from these individual ULXs in the galaxies. Compared to similar *Chandra* observations, *XMM-Newton* observations typically had substantially higher sensitivities and covered a broader energy range (0.2–15 keV), particularly important for constraining the Comptonization-related parameters. If these ULXs are indeed accreting IMBHs, they should then have lower T_{in} values than those of stellar mass BH systems (if the effect of BH spins is not important). The corresponding spectral shift of the disk emission to lower energies increases the importance of the Comptonized component in the *XMM-Newton* energy range. Therefore, *XMM-Newton* data alone may allow us to constrain simultaneously both the disk emission and the effect of the Comptonization.

Table 1 lists our selected sources with salient parameters of the host galaxies and the corresponding *XMM-Newton* observations. These six sources are located in five galaxies; each with exposure longer than 10 ksec for good counting statistics. The source positions and their offsets from galactic nuclei are listed in Table 2. All these ULXs are “persistent” sources and have been studied previously based on the data from *ASCA*, *Chandra*, and/or *XMM-Newton*.

We obtained the X-ray data from the *XMM-Newton* Science Archive and used the Standard Analysis System (SAS version 5.4.1, 2003) for data reduction, following the procedure described in the ABC guide for *XMM-Newton* Data Analysis (version 1.3, 2002). We checked light curves of individual observations and filtered out time intervals with significant contamination from soft background flares. The final effective live-time for each dataset is included in Table 1. We utilized imaging data from all three X-ray detectors: the European Photon Imaging Cameras (EPIC): MOS-1, MOS-2, and PN. The *XMM-Newton* observations of the four sources, NGC1313 X-1/X-2, IC 342 X-1, and HoIX (HolmbergIX) X-1 (sometimes referred as M81 X-9) have been reported previously, although not all of the data were used in individual studies. Observations for both NGC5408 X-1 and NGC3628 X-1 are presented here for the first time. The following is a brief summary of key results from existing work:

- NGC1313 X-1/X-2: These two ULXs have been studied by Miller et al. (2003a,b), based on the XMM-Newton MOS and PN observations, separately. From various acceptable additive two-component models, chiefly MCD+PL, they infer $T_{in} \sim 0.15$ keV for X-1 and 0.16 keV for X-2. These inferred low disk temperatures have been used as the key evidence for the consistency with the IMBH scenario. Several *ROSAT* HRI observations of these two sources show variability on the order of a factor ~ 2 (Colbert & Ptak 2002). X-1 has a radio counterpart with a luminosity of $\sim 10^{35}$ erg s $^{-1}$ (Colbert et al. 1995). An optical counterpart with R magnitude of 21.6 to X-2 has been reported by Zampieri et al. (2003). Both sources are associated with H α nebulae (Pakull & Mirioni 2003).
- IC342 X-1: This is one of the most intensively studied ULXs and has shown strong variability over the years. For example, its luminosity in 0.5 - 10 keV band was 1.3×10^{40} erg s $^{-1}$ in September 1993 (Okada et al. 1998) and decreased to 4.1×10^{39} erg s $^{-1}$ in February 2000 (Kubota, Done & Makishima 2002). The *XMM-Newton* observation, as used in the present work, displays a further decrease in the source's luminosity to 5.0×10^{39} erg s $^{-1}$. Furthermore, the source is probably associated with an SNR (Roberts et al. 2003).
- HoIX X-1: This source has been observed extensively by *Einstein*, *ROSAT*, *BeppoSAX*, and *ASCA* over 20 years. These observations show a strong time variability of the source (La Parola et al. 2001), including apparent spectral state changes. Its highest luminosity reached $\sim 1 \times 10^{40}$ erg s $^{-1}$ (Wang 2002) during an *ASCA* observation in April 1999. The source is also associated with a giant shell-like H α -emitting nebula (Wang 2002). Miller et al. (2003b) have presented an analysis of the *XMM-Newton* PN data. The T_{in} value inferred from an MCD+PL model fit is 0.21–0.26 keV, again supporting the IMBH interpretation.
- NGC5408 X-1: Kaaret et al. (2003) have reported a *Chandra* observation taken in May 2002, which indicates a luminosity of 1.1×10^{40} erg s $^{-1}$ in the 0.3–8 keV band. They have also proposed radio and optical counterparts for the source.
- NGC3628 X-1: A strong time variability has been observed from this source. Its 0.1-2 keV flux was drastically reduced by a factor of $\gtrsim 27$ between December 1991 and May 1994 (Dahlem, Heckman & Fabbiano 1995). A 52 ks *Chandra* observation in December 2000 showed a luminosity of 1.1×10^{40} erg s $^{-1}$ in the 0.3-8.0 keV band (Strickland et al. 2001). No counterpart in other wavelengths has been reported for the source.

We extracted the *XMM-Newton* spectral data from a circular region with a radius in the range of 20''–30'' around each source, depending on the source position. For each source,

the MOS-1 and MOS-2 data were combined. Each spectrum was grouped to contain a minimum 25 counts per bin. The corresponding background spectrum was taken from a concentric annulus, removing any apparent sources enclosed. A response matrix file and auxiliary response file were produced using the SAS tasks *rmfgen* and *arfgen*. The MOS and PN spectra are jointly fitted to tighten the constraints on spectral parameters.

3. Description of the CMCD Model

The construction of the CMCD model has been detailed in Paper I, including a discussion of various assumptions, comparisons with previous works, and an application to the broad-band *BeppoSAX* spectra of the stellar mass BH candidate XTE J2012+381 in our Galaxy. This application successfully removes the need for the varying inner disk radius and makes the specific predictions of both the size of the corona and the inclination angle of the accretion disk as well as a more reliable estimate of both T_{in} and R_{in} (Paper I).

We have also applied the model to the spectral analysis of the two persistent X-ray binaries, LMC X-1 and LMC X-3, which contain BH candidates (Yao et al. 2004, Paper II). Our derived foreground absorption column density (N_H) values, BH masses, and system inclinations are all consistent with those from the independent measurements based on optical and X-ray grating spectral data. These tests demonstrate the applicability and predictive capability of the CMCD model in the study of accreting BH systems.

Here we briefly describe the implementation of the CMCD model for the study of ULXs. For simplicity, we assume that the corona around the disk is spherical and that the electron energy distribution in the corona takes a thermal form, as in some previous works (e.g. Titarchuk 1994; Hua & Titarchuk 1995; Poutanen & Svensson 1996). In Paper I, we also used the "slab" geometry, which may be considered to be the opposite extreme of the spherical corona shape. However, we note that these two different geometries do not make significant differences in the fitted values of our most interested parameters (T_{in} and the model normalization). The thermal assumption is another approximation. As discussed by Coppi (1999), a more realistic electron energy distribution might be a hybrid between a thermal plasma and a non-thermal high-energy tail. The thermal part would dominate the radiative transfer process in the low energy band, whereas the non-thermal part would be important at high energies (beyond a few tens of keV). Because the *XMM-Newton* energy band used here is only upto ~ 10 keV, our results are insensitive to the deviation from the assumed thermal form.

The parameters of the CMCD model are the electron temperature (T_c), optical depth

(τ), and radius of the corona (R_c) as well as the inner disk temperature (T_{in}) and the disk inclination angle (θ). Fig. 1 illustrates the parameter dependency of the inclination angle-averaged spectra. The spectral dependency on the inclination angle is rather simple; whereas the direct soft disk emission is proportional to $\cos \theta$, the Comptonized component is not affected.

Our implementation of the CMCD model is in a standard *XSPEC* table format¹. This direct implementation avoids the unnecessary complications and approximations in constructing an analytic expression (if possible) and is convenient for any adjustments and changes in the model. The table contains a grid of spectra: T_{in} and θ values are spaced by steps of 0.1 keV and 10° linearly between the range 0.05–2 keV and between 22.7° – 79.2° , whereas T_c , τ , and R_c have 4, 7, and 4 steps evenly spaced logarithmically between 10–100 keV, 0–5, and 10–1000 R_g (where $R_g = GM/c^2$), respectively.

In a spectral fit, *XSPEC* automatically interpolates between the spectra in the table and employs a χ^2 minimization algorithm. The normalization obtained from such a fit is similar to that of the MCD model except without the cosine factor, since the disk projection effect has been taken into account in our simulation, i.e.

$$K = \left(\frac{R_{in}/\text{km}}{D/10\text{kpc}} \right)^2,$$

where D is the distance to the source and R_{in} is the apparent radius with a peak disk temperature.

We estimate the mass of each putative BH as $M = \frac{c^2 R'_{in}}{G\alpha}$, where the inner disk radius, $R'_{in} = f R_{in}$, is assumed to be the same as the last stable circular orbit radius around the BH, αR_g ($\alpha = 6$ or 1 for a non-spin or extreme spin BH). The factor $f = \eta(f_{col} f_{GR})^2 (\cos \theta / g_{GR})^{1/2}$ includes various corrections that have been dealt with in previous works (Fig. 2):

- f_{GR} and g_{GR} relate the apparent and intrinsic radii of the peak disk temperature (Zhang, Cui, & Chen 1997): f_{GR} is due to the color temperature change caused by the gravitational red shift, and Doppler shift, whereas g_{GR} is due to the integrated flux change caused by the gravitational focusing, time dilation and Doppler boosting. Both factors depend on the BH spin and θ and account for General Relativity effects. We estimate the factors from the quadratic interpolation of the tabulated values obtained by Zhang, Cui, & Chen (1997). g_{GR} and f_{GR} are in the ranges of 0.036 to 0.797 and of 0.355 to 1.657, compared to $g_{GR} = \cos(\theta)$, and $f_{GR} = 1$ in Newtonian case.

¹ftp://legacy.gsfc.nasa.gov/caldb/docs/memos/ogip_92_009/ogip_92_009.ps

- f_{col} is the spectral hardening correction factor (Ebisuzaki, Hanawa & Sugigoto 1984). Because of the high temperature at the inner disk region, which is responsible for the bulk of the emission, the inverse-Compton scattering at the surface of the disk becomes important (Ross, Fabian, & Mineshige 1992). The hardening of the spectrum effectively results in an underestimate of the inferred radius from the spectral fitting. This spectral hardening correction factor ($f_{col} = 1.7$) has been calculated by Shimura & Takahara (1995) by solving the disk structure and radiative transfer self-consistently. The above corrections give the intrinsic radius for peak disk temperature.
- η is the ratio between the R'_{in} and the intrinsic radius for peak disk temperature. We use $\eta=0.7$ (non-spin) and 0.77 (extreme spin) derived by Zhang, Cui, & Chen (1997), based on a fully relativistic calculation. In Newtonian case, $\eta = 1$.

4. Results

We summarize the results from our spectral fitting with the commonly-used MCD, PL, and MCD+PL models (Table 3) as well as the CMCD model (Table 4). The *XMM-Newton* spectra of these sources are of the highest quality available for ULXs, which allows us to test whether or not they can be characterized by these models. Table 3 shows that either PL or MCD alone can be rejected at a confidence greater than 4σ for four out of the six sources. IC 342 X-1 can be fitted reasonably well with either MCD or PL, although the latter is significantly better. The MCD model alone gives an acceptable fit to NGC3628 X-1, but the inferred T_{in} value (~ 1.9 keV) is much too high to be consistent with the IMBH interpretation. The additive MCD+PL combination is acceptable for all the sources, but it also changes the same spectral parameters drastically. For example, T_{in} for IC 342 X-1 is reduced by a factor of ~ 4 , compared to the MCD fit. Let us now compare the results in Table 3 with those from the previous studies of the individual sources:

- NGC1313 X-1/X-2: Our results on these sources are fully consistent with those from Miller et al. (2003a,b). Their results are based on the same *XMM-Newton* observations, but with MOS and PN data analyzed independently, whereas ours are obtained from the joint-fits of the data.
- IC342 X-1: Kong (2003) and Bauer et al. (2003) have shown that both PL and MCD models give satisfactory fits to the same *XMM-Newton* spectrum of this source. Our results are generally consistent with theirs. Our N_H value is slightly smaller than that obtained by Kong (2003; 5.14×10^{21} versus 6.0×10^{21} cm^{-2}), but is consistent with that from Bauer et al. (2003) within the quoted statistical errors. Such small,

though statistically significant, difference can presumably be due to various possible subtle differences in the data reduction and analysis (e.g., spectral extraction radius and binning).

- HoIX X-1: Whereas individual spectra of this source from previous X-ray observations can be modeled satisfactorily with either PL or MCD (La Parola et al. 2001; Wang 2002), these models are not acceptable for the *XMM-Newton* data. Our MCD+PL results are consistent with those reported by Miller et al. (2003b), who analyzed only the PN data. We find that the two separate observations give considerably different spectral parameters, especially the PL index. Furthermore, the luminosity of the source during these *XMM-Newton* observations is the highest known, about a factor of 2 greater than the previous record (Wang 2002).
- NGC5408 X-1: The MCD+PL model gives a marginally acceptable fit to the *XMM-Newton* spectrum. The same model was shown to be satisfactory for the *Chandra* data (Kaaret et al. 2003). Our fitted spectral parameters and the source luminosity are marginally consistent with those from Kaaret et al. (2003) within their respective uncertainties.
- NGC3628 X-1: Our obtained T_{in} for the MCD fit is higher than the value from the *Chandra* data (Strickland et al. 2001), 1.87 versus 1.38 keV. This change in T_{in} could be due to the variability of the source. However, the higher N_H value from the *Chandra* data may be due to the low-energy sensitivity degradation of the ACIS-S with time, which was apparently not corrected in the work (the correction software was only available recently).

Table 4 shows that the CMCD model fits are satisfactory (or cannot be rejected at $\gtrsim 2\sigma$ confidence) to all the sources (Fig. 3). Both N_H and T_{in} are well constrained. In particular, the T_{in} values are within a range of ~ 0.1 – 0.3 keV, although the upper limit for IC342 X-1 can reach ~ 1.3 keV. For both N_H and T_{in} values, the CMCD and MCD+PL models are consistent with each other, within the statistical uncertainties.

5. Discussions

The satisfactory fits of the CMCD model to the *XMM-Newton* spectra of our selected ULXs suggest that they are consistent with the IMBH interpretation. In particular, the model does not have the high T_{in} problem as is faced by the MCD model. The problem is apparently caused by the neglect of Comptonization in the model. Although this neglect is

statistically allowed when both the counting statistics and the energy band coverage of an observed spectrum are poor, the fitted spectral parameters are far from being physical. We conclude that the MCD model alone should not be used in the interpretation of ULXs as IMBHs.

We confirm that both T_{in} and N_H inferred from the MCD+PL model are reasonably accurate for the sources considered here. This apparent agreement between the CMCD and MCD+PL models suggests that the latter model as a whole is mathematically a good representation of the former model, at least for the IMBH candidates considered here. This is rather surprising when one considers the over-simplifications in the MCD+PL model, as discussed in §1. It appears that the nonphysical extrapolation of the PL to the low energy nearly compensates the failure to include the radiation transfer loss of soft disk photons. However, this does not mean that the MCD+PL model could be used to describe the Comptonized disk emission in general. The various nonphysical effects can cause problems for other sources, especially those with higher T_{in} values (~ 1 keV; see the discussion in §3; e.g., LMC X-1 and LMC X-3; Paper II).

In comparison, the CMCD model provides more reliable measurements of the disk parameters as well as unique constraints on the physical properties of the coronae. In the following, we briefly discuss both the function of these new parameters and the physical reason for their different degrees of constraints:

- The opacity τ is relatively well constrained, which is the key parameter that determines the total number of Comptonized photons (e.g., Fig. 4). For example, IC 342 X-1 with the largest best-fit τ value appears to have the disk emission nearly completely Comptonized, explaining why the spectrum of the source can be characterized by a PL alone. Also for this source, because the saturated Comptonization dominates over the thermal emission, the constraints on T_{in} , R_{in} , and eventually on BH mass are very weak.
- The corona electron temperature T_c is chiefly responsible for the overall energy extent of the Comptonized spectral component. Because T_c is $\gtrsim 30$ keV for all the sources, the high-energy turning-off of the component is well beyond the *XMM-Newton* band limit. Therefore, the data do not constrain the upper limit of T_c . The lower limit is determined because a minimum electron energy is needed to up-scatter soft disk photons to the high energies covered by the spectra.
- Whereas the nearly isotropic Comptonized flux is barely affected by the disk inclination angle θ , the observed strength of the soft disk component is proportional to $\cos(\theta)$. In a spectral fit, however, this difference in the disk inclination dependence may be partially

compensated by a change in the τ value. But if θ is large (for a nearly edge-on disk), its geometric effect cannot be canceled by adjusting other parameters, which would also effectively alter the spectral shapes of both the disk and Comptonized components in a spectral fit (e.g., Fig. 4). Consequently, we may constrain the upper limit to θ . This constraint, though not very tight, is important for the estimation of the BH masses (§3).

- R_c determines the effective corona radius, within which the disk emission is most affected by the Comptonization. Photons from larger radii have relatively little chance to be scattered and may contribute to the un-Comptonized disk component even if τ is large (≥ 1). But the amount of soft X-ray radiation from the disk also decreases with the increasing radius. The combination of these two effects may thus place a constraint on R_c .

Apparently, these parameters are correlated in a spectral fit. This, together with the limited counting statistics and bandwidth of the data, explains why the parameters are not tightly constrained. Nevertheless, the results presented above demonstrate the potential of the CMCD model to shed new insights into the physical properties of the accretion disk coronae, in addition to a more reliable mass estimate of the putative BHs.

Table 5 includes our estimated BH masses, assuming no spin and the best-fit θ values. The typical BH mass is in the range of $\sim 10^3 - 10^4 M_\odot$, although the upper limit for IC 342 X-1 is slightly higher. If a BH spins rapidly, the inferred BH mass could be several times higher than the value quoted in the table (depending on θ ; Fig. 2).

Assuming that the bolometric luminosity (estimated in the 0.05–100 keV range) $L_{bol} = 0.1\dot{M}c^2$, we further estimate the accretion rate \dot{M} for each source (Table 5), which is in the range of $1-10 \times 10^{-6} M_\odot \text{yr}^{-1}$.

The present work represents, at most, an incremental step in developing a fully self-consistent model for accreting BH systems. The CMCD model used here deals only with the Comptonization by static disk coronae. To study the dynamics, one needs to understand the formation and evolution of the coronae as well as the physics of the accretion disks. We also have not considered other proposed scenarios that may explain some of the ULXs; e.g., the anisotropic emission of the radiation (King et al. 2001), the relativistic motion of the X-ray-emitting plasmas (Fabrika & Mescheryakov 2001), and the possible super-Eddington emission (Begelman 2002). Spectral models for such scenarios, yet to be developed, need to account for the apparent presence of the soft thermal component, in addition to the power law, for these sources except in the case of IC 342 X-1. The bottom line here is that the *XMM-Newton* spectra are consistent with the IMBH interpretation of the sources.

We thank Xiaoling Zhang for useful discussions and the referee for many thoughtful comments that helped in improving the presentation of the paper. This work is supported by the NASA LTSA grant NAG5-8935.

REFERENCES

- Arnaud, K. A. 1996, in *Astronomical Data Analysis Software and Systems V* (ASP Conf. Series volume 101), eds. Jacoby G. and Barnes J., p17
- Bauer, F. E., Brandt, W. N., & Lehmer, B. 2003, *AJ*, 126, 2797
- Begelman, M. C. 2002, *ApJ*, 568, L97
- Campana, S., et al. 2002, *A&A*, 382, 163
- Colbert, E. J. M., et al. 1995, *ApJ*, 446, 177
- Colbert, E. J. M. & Mushotzky, R. F. 1999, *ApJ*, 519, 89
- Colbert, E. J. M. & Ptak, A. F. 2002, *ApJ*, 143, 25
- Coppi, P. S. 1999, Invited review at the workshop “High Energy Processes in Accreting Black Holes”, eds. J. Poutanen and R. Svensson, ASP Conf. Series, Vol. 161, p. 375 (astro-ph/9903158)
- Cropper, M. et al. 2003, *MNRAS*, in press (astro-ph/0311302)
- Dahlem, M., Heckman, T. M., & Fabbiano, G. 1995, *ApJ*, 442, L49
- Dickey, J. M. & Lockman, F. J. 1990, *ARA&A*, 28, 215
- Ebisuzaki, T., Hanawa, T. & Sugigoto, D. 1984, *PASJ*, 36, 551
- Fabbiano, G. 1989, *ARA&A*, 27, 87
- Fabrika, S. & Mescheryakov, A. 2001, to be published in *High Angular Resolution in Astronomy*, ed. R. Schilizzi et al. , (ASP Publication) (astro-ph/0103070)
- Freedman, W. L., et al. 1994, *ApJ*, 427, 628
- Hua, X.-M. & Titarchuk, L. 1995, *ApJ*, 449, 188
- Kaaret, P., et al. 2003, *Science*, 299, 365

- Karachentsev, I. D., et al. 2002, *A&A*, 385, 21
- King, A. R., et al. 2001, *ApJ*, 552, 109
- Kong, A. K. H. 2003, *MNRAS*, 346, 265
- Kubota, A., Makishima, K., & Ebisawa, K. 2001, *ApJ*, 560, L147
- Kubota, A., Done, C., & Makishima, K. 2002, *MNRAS*, 337, 11
- La Parola, V., et al. 2001, *ApJ*, 556, 47
- Makishima, K., et al. 1986, *ApJ*, 308, 635
- Makishima, K., et al. 2000, *ApJ*, 535, 632
- Miller, M. C., & Colbert, E. J. M. 2003, *Modern Physics D.*, in press (astro-ph/0308402)
- Miller, J. M., Fabbiano, G., Miller, M.C., & Fabian, A. C. 2003a, *ApJ*, 585, L37
- Miller, J. M., Fabian, A. C. & Miller, M.C. 2003b, *ApJ*, submitted (astro-ph/0310617)
- Okada, K., et al. 1998, *PASJ*, 50, 25
- Page, M. J., et al. 2003, *MNRAS*, 345, 639
- Pakull, M. W., & Mirioni, L. 2003, *RevMexAA*, 15, 197
- Poutanen, J., & Svensson, R. 1996, *ApJ*, 470, 249
- Roberts, T. P., et al. 2003, *MNRAS*, 342, 709
- Ross, R. R., Fabian, A. C., & Mineshige, S. 1992, *MNRAS*, 258, 189
- Saha, A., Claver, J., & Hoessel, J. G. 2002, *ApJ*, 124, 861
- Shimura, T., & Takahara, F. 1995, *ApJ* 445, 780
- Soifer, B. T., et al. 1987, *ApJ*, 320, 238
- Strickland, D. K., et al. 2001, *ApJ*, 560, 707
- Strohmayer, T. E., & Mushotzky, R. F. 2003, *ApJ*, 586, L61
- Titarchuk, L. 1994, *ApJ*, 434, 570
- Tully, R. B. 1988, *Nearby Galaxies Catalog* (Cambridge Univ. Press)

- van der Marel, R. P. 2003, in *Carnegie Observatories Astrophysics Series, Vol. 1: Coevolution of Black Holes and Galaxies*, ed. L. C. Ho (Cambridge: Cambridge Univ. Press), 2003, in press (astro-ph/0302101)
- Wang, Q. D. 2002, *MNRAS*, 332, 764
- Yao, Y. et al. 2003, *ApJ*, submitted (astro-ph/0303535) (Paper I)
- Yao, Y. et al. 2004, in preparation (Paper II)
- Young, J. S., & Scoville, N. Z. 2002, *ARA&A*, 29, 531
- Zampieri, L., et al. 2003, *Proc. of the BeppoSAX Symposium: “The Restless High-Energy Universe”* (Amsterdam, May 5-8, 2003), E.P.J. van den Heuvel, J.J.M. in 't Zand, and R.A.M.J. Wijers (Eds), *Nucl. Physics B. Suppl. Ser.*, Elsevier (astro-ph/0309687)
- Zhang, S. N., Cui, W., & Chen, W. 1997, *ApJ*, 482, L155

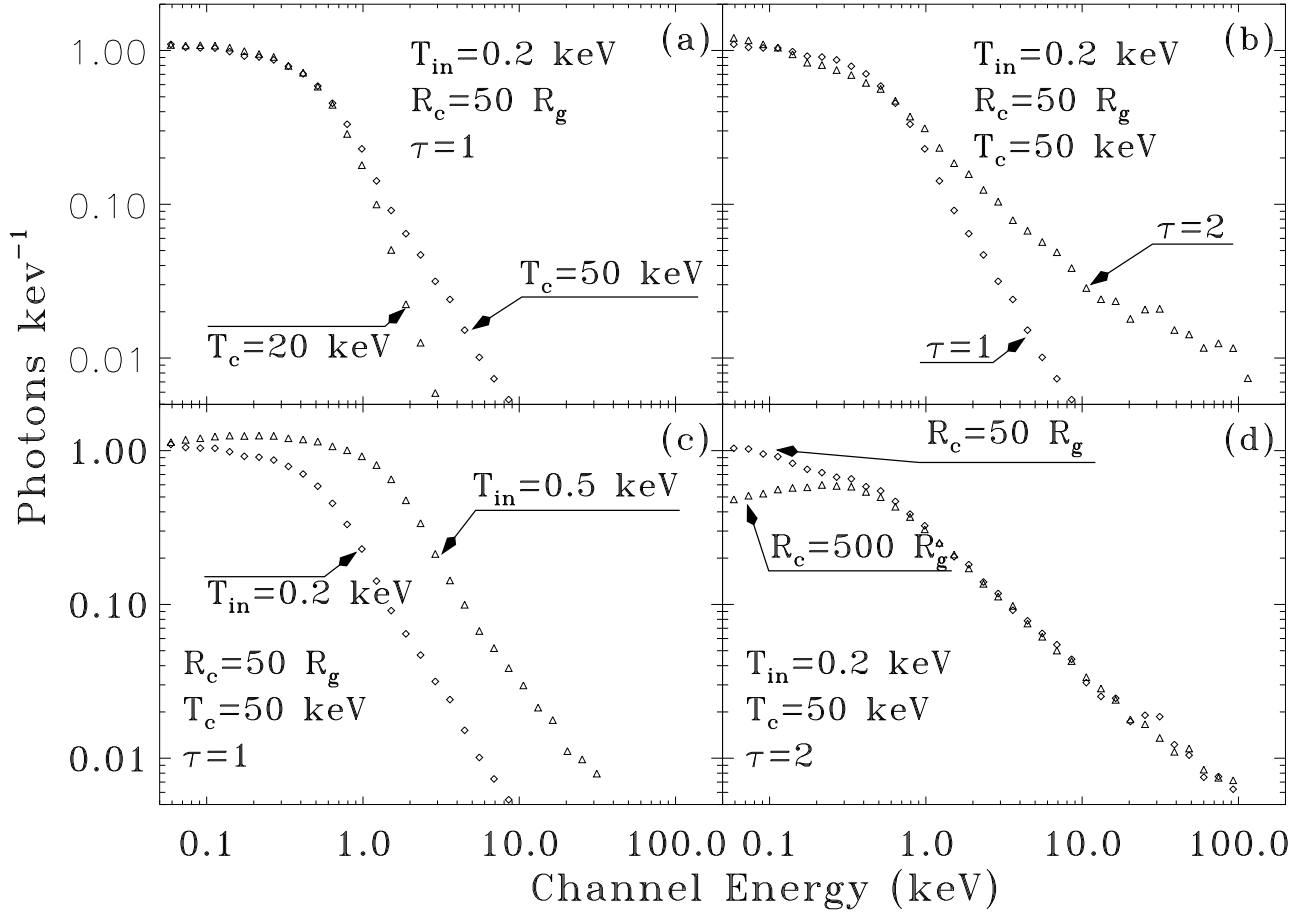


Fig. 1.— Spectral dependencies on the electron temperature T_c (a), opacity of the corona τ (b), inner disk temperature T_{in} (c) and the corona size R_c (d). Definitions of the listed parameters are given in the text.

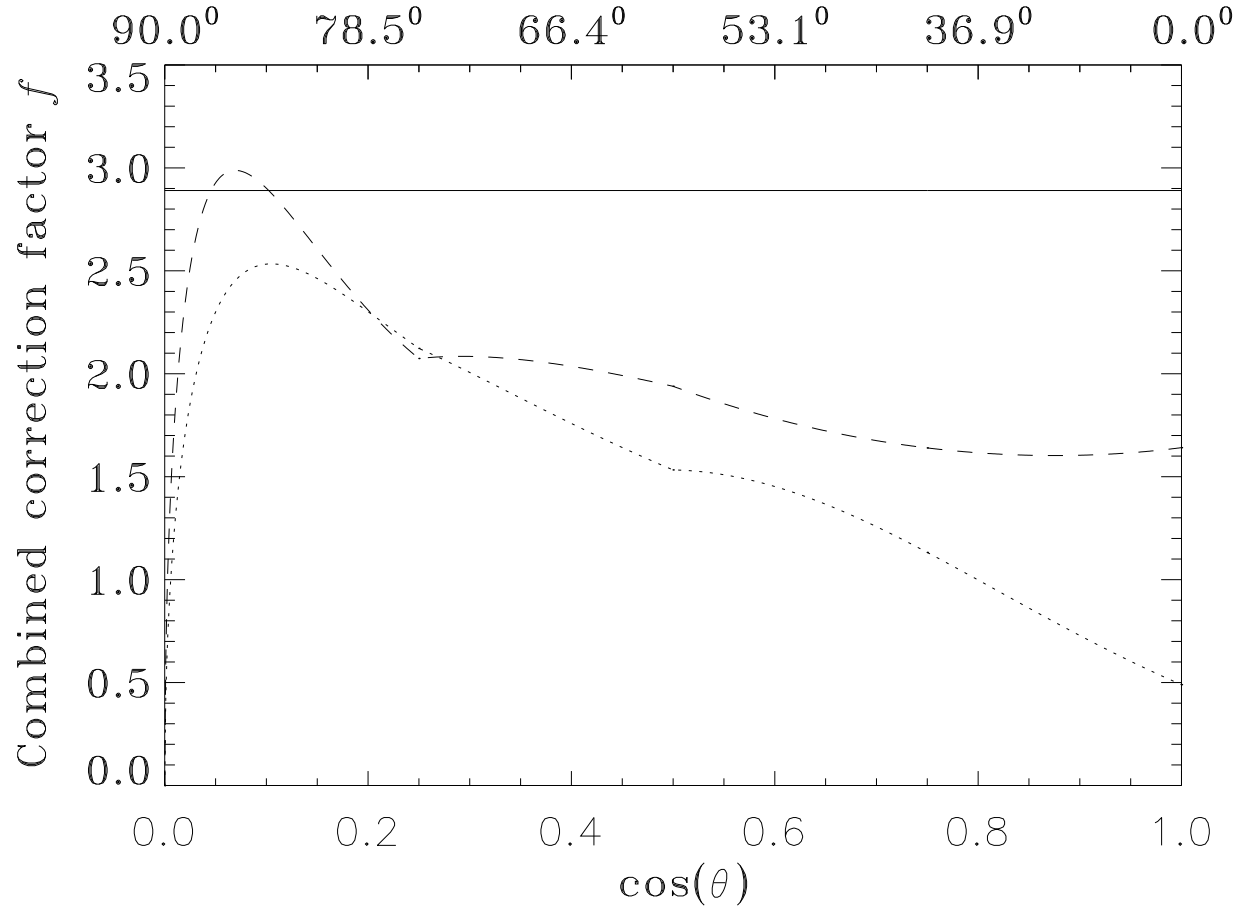


Fig. 2.— The combined R_{in} correction factor f vs. the disk inclination angle θ (the scale at the top), or $\cos(\theta)$ (at the bottom). *Solid line*: Newtonian case; *dashed line*: non-spin case; and *dotted line*: extreme spin case. The figure is based on Table 1 of Zhang, Cui, & Chen (1997).

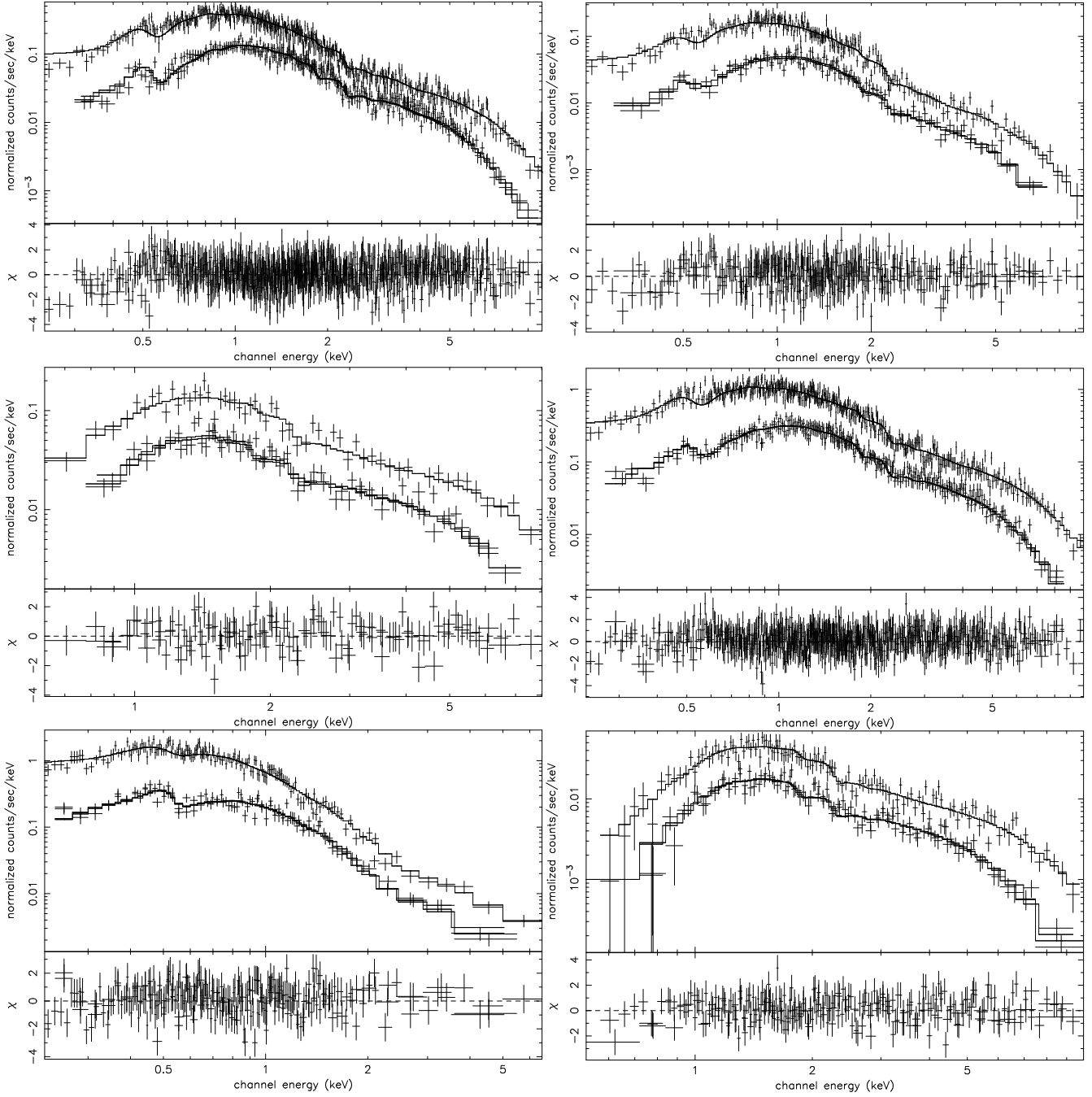


Fig. 3.— Model fits to the *XMM-Newton* spectra of ULXs: NGC1313 X-1 (top left), NGC1313 X-2 (top right), IC342 X-1 (middle left), HoIX X-1 (OBS 1 only for clarity; middle right), NGC5408 X-1 (bottom left), and NGC3628 X-1 (bottom right). The solid line shows the fit of the CMCD model. For each source, the model is jointly applied to the PN spectrum (which always has a higher flux) as well as to the MOS 1 & 2 spectra.

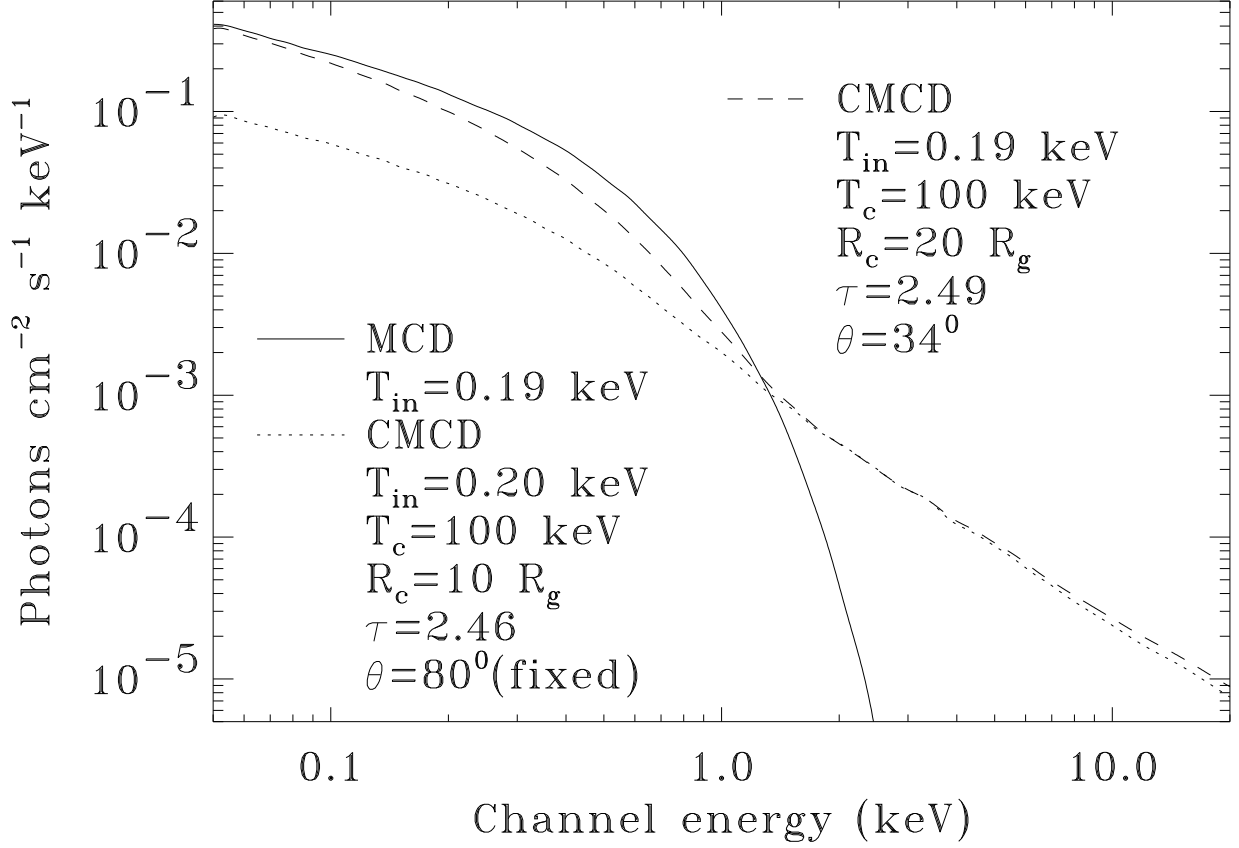


Fig. 4.— Illustration of the spectral dependence on the corona opacity τ and disk inclination θ in the MCD model of HoIX X-1: the absorption-corrected best-fit CMCD model (*dashed line*); the corresponding MCD model before Comptonization (*solid line*); the absorption-corrected best-fit CMCD model with inclination fixed at $\theta = 80^{\circ}$ (*dotted line*).

Table 1. Selected ULXs and *XMM-Newton* Observations

Galaxy	Hubble Type	D (Mpc)	N_{HI} (10^{21}cm^{-2})	OBS ID	OBS Date (mm/dd/yy)	MOS1 (ksec)	MOS2 (ksec)	PN (ksec)	Filter
NGC1313 X-1/X-2	SB(s)d	3.7	0.40	0106860101	10/17/00	28.9/29.3	28.9/29.2	28.4/31.6	medium
IC342 X-1	Scd	3.3	3.03	0093640901	02/11/01	9.5/9.8	9.5/9.8	5.0/5.9	medium
HoIX X-1	Im	3.6	0.40	0112521001	04/10/02	10.0/10.1	10.0/10.1	6.8/7.8	thin1
(or M81 X-9)				0112521101	04/16/02	7.9/10.8	7.9/10.8	7.4/8.5	thin1
NGC5408 X-1	IB(s)m	4.8	0.57	0112290601	08/08/01	5.9/7.5	5.9/7.5	4.2/5.0	thin1
NGC3628 X-1	Sbc	10.0	0.22	0110980101	11/27/00	42.2/54.5	42.3/54.6	32.2/50.7	thin1

Note. — D is the galaxy distance: NGC1313 (Tully 1988), IC342 (Saha, Claver, & Hoessel 2002), HoIX (Freedman et al. 1994), NGC5408 (Karachentsev et al. 2002), and NGC3628 (Soifer et al. 1987), whereas the N_{HI} values are all from the Galactic HI survey by Dickey & Lockman (1990). Exposure time of MOS1, MOS2, and PN are listed as the cleaned time interval used for our analysis/original exposure time.

Table 2. Positions of the Selected ULXs

ULXs	R.A. (J2000)	Dec. (J2000)	δ (')
NGC1313 X-1	3:18:20.21	-66:29:10.7	0.83
NGC1313 X-2	3:18:22.62	-66:36:05.9	6.2
IC342 X-1	3:45:55.46	68:04:54.2	5.0
HoIX X-1	9:57:53.50	69:03:47.8	2.2
NGC5408 X-1	14:03:19.62	-41:23:00.2	0.42
NGC3628 X-1	11:20:16.23	13:35:15.0	0.12

Note. — The X-ray source positions are from the *XMM-Newton* observations, whereas δ is the projected offset of each source position from the respective galactic center obtained from NED.

Table 3: Results from spectral fits with the PL, MCD, and PL+MCD models

Source	Model	N_H (10^{21} cm $^{-2}$)	Γ_p or T_{in} (keV)	K_{PL} or K_{MCD}	χ^2/dof
NGC1313 X-1	PL	2.11 (2.03–2.19)	1.95 (1.92–1.98)	6.3×10^{-4}	1222/783
	MCD	0.49 (0.44–0.53)	1.39 (1.36–1.43)	0.031	2217/783
	PL+	4.43(4.00–4.86)	1.81(1.78–1.85)	5.51×10^{-4}	851/781
	MCD		0.16(0.15–0.18)	628	
NGC1313 X-2	PL	2.82 (2.68–2.97)	2.51 (2.44–2.57)	4.4×10^{-4}	474/352
	MCD	0.78 (0.70–0.87)	0.85 (0.81–0.88)	0.092	858/352
	PL+	3.72 (3.14–4.41)	2.23(2.14–2.36)	3.3×10^{-4}	386/350
	MCD		0.18(0.16–0.20)	99	
IC342 X-1	PL	5.13 (4.56–5.75)	1.66 (1.57–1.76)	5.4×10^{-4}	113/129
	MCD	2.76 (2.39–3.16)	1.91 (1.77–2.08)	0.011	146/129
	PL+	5.14 (3.82–9.19)	1.54 (0.78–1.76)	4.5×10^{-4}	112/127
	MCD		0.50 (0.10–0.93)	0.23	
HoIX X-1 obs.1	PL	1.81(1.73–1.89)	1.86(1.83–1.89)	17×10^{-4}	852/707
	MCD	0.37(0.32–0.41)	1.46(1.42–1.50)	0.08	1593/707
	PL+	2.90(2.55–3.27)	1.72(1.66–1.74)	14×10^{-4}	706/705
	MCD		0.20(0.18–2.23)	220	
HoIX X-1 obs.2	PL	2.14(2.07–2.22)	1.94(1.91–1.97)	22×10^{-4}	937/ 769
	MCD	0.57(0.52–0.61)	1.38(1.35–1.42)	0.11	1764/769
	PL+	3.49(3.08–3.94)	1.86(1.82–1.91)	20×10^{-4}	810/767
	MCD		0.17(0.16–0.19)	689	
NGC5408 X-1	PL	1.96 (1.80–2.15)	3.79 (3.67–3.93)	13×10^{-4}	393/260
	MCD	0.40 (0.32–0.49)	0.30 (0.29–0.31)	21	640/260
	PL+	1.34(1.15–1.65)	2.56(2.36–2.81)	4.7×10^{-4}	283/258
	MCD		0.18(0.16–0.19)	285	
NGC3628 X-1	PL	6.77 (6.26–7.32)	1.78 (1.71–1.86)	1.6×10^{-4}	298/246
	MCD	3.84 (3.52–4.18)	1.87 (1.77–1.99)	0.003	398/246
	PL+	9.53(7.54–11.9)	1.74(1.58–1.89)	1.6×10^{-4}	285/244
	MCD		0.23(0.18–0.36)	15	

Note. — Γ_p is the photon index of the PL model. The normalization of the PL model, K_{PL} , is defined as photons keV $^{-1}$ cm $^{-2}$ s $^{-1}$ at 1 keV, whereas the normalization of the MCD model, K_{MCD} , is defined as $(R_{in}/\text{km})^2 \cos\theta / (D/10 \text{ kpc})^2$. The uncertainty ranges of the parameters are all at the 90% confidence.

Table 4: Results from spectral fits with the CMCD model

Source	$N_H(10^{21} \text{ cm}^{-2})$	$T_{in}(\text{keV})$	$T_c(\text{keV})$	$R_c(R_g)$	τ	θ (deg)	$K(10^2)$	χ^2/dof
NGC 1313 X-1	4.11(3.98,4.27)	0.199(0.159,0.201)	100(95,-)	11(-,15)	2.7(2.4,3.1)	23(-,34)	3.4(3.1,6.5)	860/779
NGC 1313 X-2	3.25(3.09,3.73)	0.19(0.12,0.20)	99(68,-)	49(24,84)	1.0(0.87,1.4)	23(-,58)	1.3(0.89,3.1)	381/348
IC342 X-1	5.23(4.13,6.53)	0.32(0.05,1.27)	49(28,-)	20(-,-)	5.0(2.3,-)	79(-,-)	0.57(0.01,49)	111/125
HoIX X-1 obs.1	3.35(3.12,3.57)	0.19(0.12,0.20)	100(76,-)	19(10,28)	2.5(2.2,3.1)	34(-,59)	8.8(5.5,35)	710/703
HoIX X-1 obs.2	3.31(3.08,3.67)	0.18(0.10,0.20)	100(69,-)	22(-,41)	1.9(1.7,3.4)	50(-,62)	12(6.6,52)	816/765
NGC5408 X-1	1.31(1.19,1.39)	0.13(0.11,0.20)	98(66,-)	10(-,17)	1.0(0.81,1.4)	25(-,53)	9.5(2.1,27)	279/256
NGC3628 X-1	9.79(7.97,11.85)	0.21(0.12,0.31)	100(33,-)	22(-,42)	2.6(2.1,-)	23(-,73)	0.49(0.1,4.7)	283/242

Note. — The upper limit of our current table model for T_c is 100 keV. The symbol ‘-’ indicates that the limit is not constrained.

Table 5: Inferred Parameters from the CMCD Model

Source	$f_{2-10}/f_{0.2-10}$	$L_{2-10}/L_{0.2-10}$	$\log(R'_{in}/\text{km})$	$\log(M_{\text{BH}}/M_{\odot})$	\dot{M}/\dot{M}_6
NGC1313 X-1	1.9/9.1	3.1/14.8	4.04(4.02,4.20)	3.09(3.08,3.25)	4.9
NGC1313 X-2	0.6/2.8	1.0/4.6	3.83(3.76,4.06)	2.88(2.81,3.11)	1.2
IC342 X-1	2.4/4.1	3.1/5.4	3.77(3.48,5.41)	2.82(2.53,4.46)	3.1
HoIX X-1 (OBS 1)	5.7/19.5	8.8/30.3	4.23(4.14,4.63)	3.29(3.20,3.68)	11.3
HoIX X-1 (OBS 2)	6.3/20.8	9.8/32.2	4.33(4.22,4.76)	3.38(3.28,3.81)	10.2
NGC5408 X-1	0.6/7.1	1.6/19.6	4.38(4.16,4.66)	3.43(3.21,3.71)	5.0
NGC3628 X-1	0.6/2.1	7.3/25.3	4.05(3.83,4.78)	3.10(2.88,3.83)	9.7

Note. — The fluxes f_{2-10} and $f_{0.2-10}$ have been corrected for the absorption and are in units of 10^{-12} erg cm $^{-2}$ s $^{-1}$ and are in the energy range 2–10 and 0.2–10 keV, respectively. The luminosities L_{2-10} and $L_{0.2-10}$ are in units of 10^{39} erg s $^{-1}$ and are calculated from the fluxes and the distances in Table 1. The \dot{M}_6 is 10^{-6} M $_{\odot}$ yr $^{-1}$. Assuming no spin and $L_{bol} = 0.1\dot{M}c^2$. See text for detail.